IOPscience iopscience.iop.org

Home Search Collections Journals About Contact us My IOPscience

Synthesis of Fe–Al nanoparticles by hydrogen plasma–metal reaction

This article has been downloaded from IOPscience. Please scroll down to see the full text article.

2003 J. Phys.: Condens. Matter 15 2507

(http://iopscience.iop.org/0953-8984/15/17/306)

View the table of contents for this issue, or go to the journal homepage for more

Download details:
IP Address: 171.66.16.119
The article was downloaded on 19/05/2010 at 08:48

Please note that terms and conditions apply.

INSTITUTE OF PHYSICS PUBLISHING JOURNAL OF PHYSICS: CONDENSED MATTER

J. Phys.: Condens. Matter **15** (2003) 2507–2513 PII: S0953-8984(03)59437-1

Synthesis of Fe–Al nanoparticles by hydrogen plasma–metal reaction

Tong Liu, Huaiyu Shao and Xingguo Li

The State Key Laboratory of Rare Earth Materials Chemistry and Applications, Peking University, Beijing 100871, China

Received 7 February 2003
Published 22 April 2003
Online at stacks.iop.org/JPhysCM/15/2507

Abstract

Fe–Al nanoparticles of eight kinds have been prepared by hydrogen plasma–metal reaction. The morphology, crystal structure, and chemical composition of the nanoparticles obtained were investigated by transmission electron microscopy (TEM), x-ray diffractometry (XRD), and induction-coupled plasma spectroscopy. The particle size was determined by TEM and Brunaumer–Emmet–Teller gas adsorption. It was found that all the nanoparticles have spherical shapes, with average particle size in the range of 29–46 nm. The oxide layer in nanoparticles containing Al after passivation is not observable by XRD and TEM. The Al contents in Fe–Al ultrafine particles are about 1.2–1.5 times those in the master alloys. The evaporation speeds of Al and Fe in Fe–Al alloys are mutually accelerated at a certain composition. The crystal structures of the Fe–Al nanoparticles vary with the composition of the master alloys. Pure $Fe_3Al(D0_3)$ and FeAl (B2) structures are successfully produced with 15 and 25 at.% Al in bulks, respectively. For samples of Fe–Al nanoparticles with Al content over 56.5 at.%, the crystal structures of the nanoparticles do not comply with the equilibrium phase diagram and there is no intermetallic formation except that of Fe_3Al and FeAl.

1. Introduction

Metallic nanoparticles are of great interest due to their unique properties and a wide range of potential applications including in information storage, catalysis, and hydrogen storage, and as permanent magnets and ferrofluids [1–4]. Nanoparticles of pure metals and alloys have been reportedly produced by chemical reduction, hydrolysis, sputtering, inert gas condensation, hydrogen plasma–metal reaction (HPMR), and so on [5–9]. HPMR, a newly developed method, is suitable for preparing ultrafine particles (UFPs) of various metals or alloys industrially. Several less reactive metals and alloys such as Fe, Ni, Co and their alloys have been fabricated by HPMR, and the mechanism of formation of UFPs is extensively studied [10–14]. Recently, we have investigated the synthesis of Ti–Fe nanoparticles by HPMR, intending to synthesize

 © 2003 IOP Publishing Ltd Printed in the UK

Fe–Ti intermetallic nanoparticles [15]. Since Ti and FeTi intermetallics can adsorb hydrogen, no pure intermetallic metal nanoparticles were formed.

Iron aluminide intermetallics constitute a relatively new class of materials that provide the advantages of good mechanical properties, light weight, and good corrosion resistance. As important intermetallics, they have great potential for applications in automobile engines, aircraft, and electricity generation and energy conversion equipment. To overcome some of the shortcomings, e.g. brittle fracture and low ductility at ambient temperature, recently considerable efforts have been made in an attempt to synthesize and characterize nanocrystalline Fe–Al intermetallics by mechanical alloying (MA) [16–18]. However, there is a lack of research on the preparation of Fe–Al intermetallic compound nanoparticles, which have many potential uses, particularly in the field of magnetics for bar-coding and magnetic ink applications. Al and iron aluminides do not absorb hydrogen, and there are several intermetallic compounds in the Fe–Al system. It therefore looks very promising to produce pure iron aluminides by HPMR. In this study, we intend to prepare pure Al–Fe intermetallic compound nanoparticles by HPMR, and investigate their structures and characteristics.

2. Experimental details

A schematic illustration of the experimental equipment used for synthesis of nanoparticles by HPMR was given previously [11]. The equipment is primarily composed of an arc-melting chamber and a collecting system. The bulk Fe–Al ingots were prepared from 99.9% purity Fe and Al by arc melting in an argon gas atmosphere. Arc-melted ingots were flipped over and remelted four times to get a homogeneous composition. Then Fe–Al nanoparticles were produced by arc melting each of the Fe–Al ingots in a 50% Ar and 50% H_2 (by volume) mixture of 0.1 MPa. The flow rate of the circulation gas for collection of nanoparticles is 100 l min^{-1}. Since the rate of production of UFPs is affected by master sample mass, identical master alloy buttons weighing 50 g were used in this work. The arc current and voltage were selected as 300 A and 25 V, respectively. Eight master Fe–Al alloys containing 0, 5, 15, 25, 30, 50, 70, 100 at.% Al were used. After passivation in a 95% Ar + 5% O_2 (by volume) atmosphere for 24 h, the nanoparticles were taken out of the arc-melting chamber. The crystal structure of the as-prepared nanoparticle samples was characterized by x-ray diffractometry (XRD) using monochromatic Cu Kα radiation. The morphology, size distribution, and shape of particles were observed by transmission electron microscopy (TEM) using a 200 kV JEOL EX microscope. The Brunaumer–Emmet–Teller specific surface areas of nanoparticles were measured by means of N_2 adsorption using a Counter SA 3100 volumetric gas adsorption analyser and the average particle size was evaluated. The composition of the UFPs was determined by an induction-coupled plasma (ICP) spectrophotometer.

3. Results and discussion

Figure 1 shows the relationship between the chemical compositions of the Fe–Al nanoparticles and the master alloys. The compositions of Fe–Al UFPs are different from those of the master Fe–Al alloys. For the master alloy containing 5, 15, 25, 30, 50, 70 at.% Al, there is 5.9, 27.1, 46.1, 56.5, 84.1, 96.3 at.% Al, respectively, in the UFP samples. This can be explained using Ohno and Uda's equation [9]: the generation speed for pure Al estimated from this equation is about double that for pure Fe. In fact, the Al contents in Fe–Al UFPs are about 1.2–1.7 times those in the master alloys. It is found that the content of Al in the nanoparticles varies almost directly with the content of Al in the master alloy below 50 at.%. For convenience, hereafter the

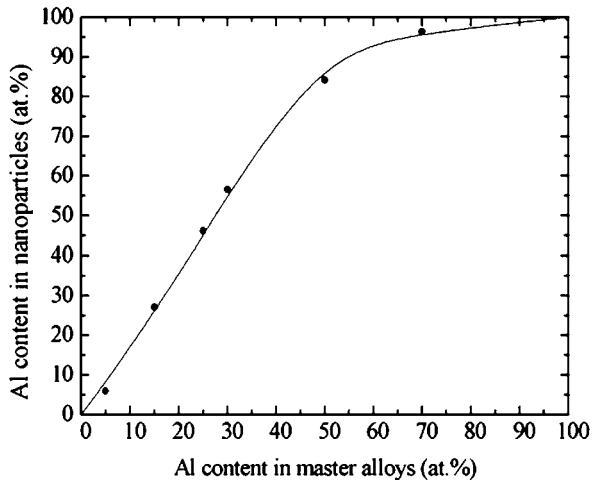

Figure 1. The relationship between the Al contents in the Fe–Al nanoparticles and master alloys.

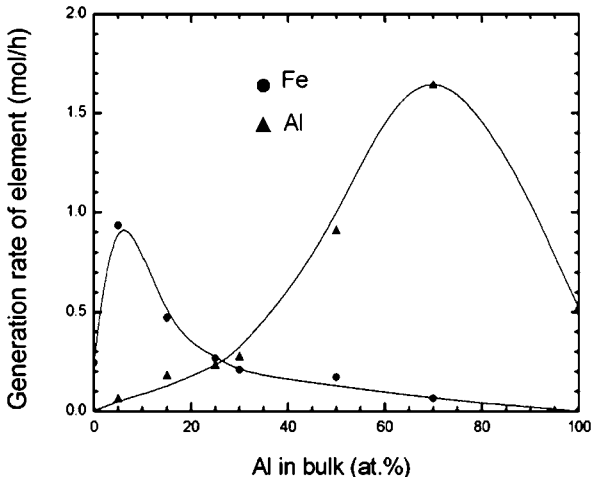

Figure 2. Speeds of generation of Al and Fe by HPMR.

samples are referred as (a) Fe, (b) Fe—5.9 at.% Al, (c) Fe—27.1 at.% Al, (d) Fe—46.1 at.% Al, (e) Fe—56.5 at.% Al, (f) Fe—84.1 at.% Al, (g) Fe—96.3 at.% Al, and (h) Al.

Figure 2 shows the generation speeds for Al and Fe at different Al contents in master alloy. It is interesting to find that with Al concentrations in the master alloy increasing from 0 to 25 at.%, the speed of evaporation of Fe in Al–Fe alloy is larger than that for pure Fe. The speed of evaporation of Fe with 5 at.% Al in the master alloy is about four times that of pure Fe. Similarly, with the Al content larger than 50 at.%, the speed of evaporation of Al in the Fe–Al alloy is higher than that for pure Al. The speed of evaporation of Al with 70 at.% Al in the master alloy is about three times that for the pure Al sample. As the Al content varies from 25 to 100 at.%, the generation speed for Fe declines gradually. The generation speed for Al in Al–Fe alloy increases but at a low rate with Al ranging from 0 to 30 at.% in the master alloy. Between 30 and 70 at.% Al, the speed of generation of Al increases greatly. It is well known that the melting point of the alloy is lower than that of the pure metal, but the

Table 1. Characteristics of Al–Fe UFP samples.

Samples	Composition of Al (at.% in bulk alloy)	Composition of Al (at.% in UFPs)	Specific surface area ($m^2\ g^{-1}$)	Mean particle size (nm)	Phase in UFPs
(a)	0	0	23.6	32	Fe (bcc)
(b)	5	5.9	24.5	40	Fe (bcc)
(c)	15	27.1	26.0	38	Fe_3Al ($D0_3$)
(d)	25	46.1	34.3	35	FeAl (B2)
(e)	30	56.5	44.9	29	FeAl (B2) + Fe (bcc)
(f)	50	84.1	62.2	30	Al (fcc) + unidentified
(g)	70	96.3	46.5	43	Al (fcc)
(h)	100	100	48.3	46	Al (fcc)

boiling points of each of the metals in the alloy do not change in that way. Supposing that the plasma energies are equal for all alloy samples, the rate of evaporation of Al or Fe in the Fe–Al alloys should be lower than that for pure Al or Fe since the heating area for Al and Fe in pure metal is higher than that in the alloy. However, it is indicated from our work that Fe and Al accelerate the evaporation of Al and Fe in Fe–Al UFPs at a certain scale of composition; this has seldom been reported for other bimetallic UFPs prepared by HPMR. This cannot be explained by Ohno and Uda's theory [9]. It is proposed that the addition of Al in Fe (or Fe in Al) might change the interaction of metals and hydrogen, and the metal evaporates more easily in some compositions of alloy than in the pure metal. The detailed mechanism of these interesting phenomena has not yet been determined, and further study is now in progress.

It is noted that the particles produced by aerosol methods are essentially in a Gaussian distribution [19]. In this work, the nanoparticles of all the samples are spherical in shape and have a size distribution ranging from about 5 to 100 nm in diameter, with the mean diameters in the range of about 30–40 nm, as shown in figure 3. It is found that samples (g) and (h) with high Al content have larger particle size than other samples due to the high rate of generation of Al, leading to more coalescence during the cooling process. However, there is no clear relationship between the mean particle size and composition of Fe–Al nanoparticles with low Al content. A thin layer several nanometres in thickness appears in sample (a), which is found to be iron oxide by XRD. No layers are formed in nanoparticles containing Al. The specific surface areas of the Fe–Al nanoparticles vary from 23.6 to 62.2 $m^2\ g^{-1}$, as summarized in table 1. The mean particle diameters for all samples predicted from the specific surface area are in the range of 29–46 nm, in good agreement with the results from TEM.

Figure 4 shows the XRD patterns of the as-prepared UFP samples, and the crystal structures are shown in table 1. A weak peak around 35.4° is noticeable for pure Fe (bcc) nanoparticles, in figure 4(a), suggesting the presence of a small amount of iron oxide. Typically, the UFP samples oxidize slightly after a suitable surface treatment before being exposed to air, as in the cases of other metallic UFPs [20]. For the samples containing Al in figure 4, however, there is no iron oxide detectable in the XRD patterns. It seems that the addition of Al increases the oxidation resistance of the nanoparticles. It can be determined from figure 4 that samples (a) and (b) have the structure of α-Fe (bcc), and samples (g) and (h) have that of Al (fcc). As regards samples (c) and (d), pure Fe_3Al (($D0_3$)) and FeAl (B2) intermetallics are successfully produced. Both intermetallics and metals are found in samples (e) and (f).

The formation of the UFPs from Fe–Al binary alloy can be explained as follows. First, Fe and Al vapours form under H_2 and Ar plasma simultaneously. Fe and Al vapours then begin to condense and solidify. As non-hydrogen-absorbing metals, they do not react with hydrogen

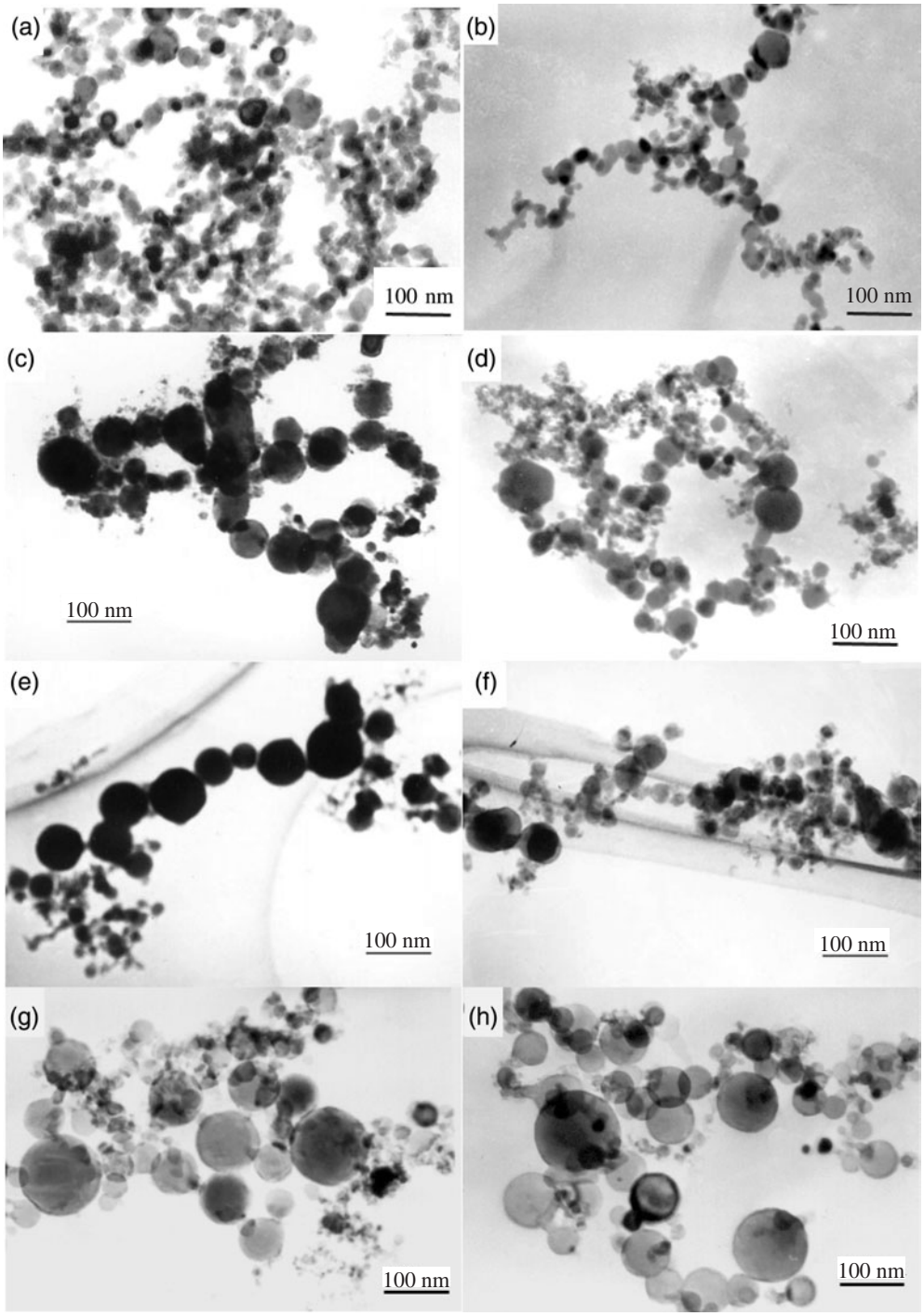

Figure 3. TEM bright-field images of samples (a)–(h).

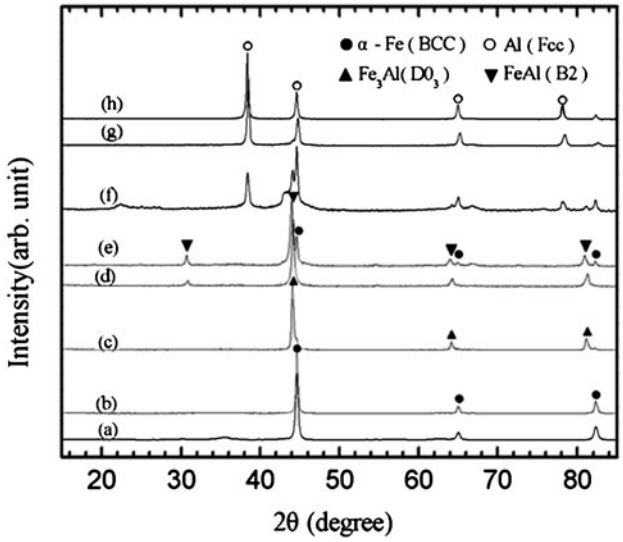

Figure 4. XRD patterns of samples (a)–(h).

during vaporization and cooling processes. During the condensation stage, Al atoms collide with Fe atoms and begin to condense in the same metal cluster and then grow into nanoparticles. It is seen from the Fe–Al phase diagram [21] that the Al solid solubility limit in α-Fe goes as high as 47 at.% at 1583 K. α-Fe (bcc) exists between 1583 and 298 K in the equilibrium phase transformation for Fe–5.9 at.% Al. The nanoparticles produced in sample (b) therefore retain the α-Fe structure even at high cooling rates. For sample (c), containing 27.1 at.% Al, α-Fe occurs between 1773 and 1123 K, and the pure $D0_3$ structure of iron aluminide should be synthesized finally at room temperature. However, during HPMR processing, the cooling rate goes as high as 10^5 K s^{-1}, so α-Fe is unable to transform into the $D0_3$ structure fully, and a small amount of α-Fe still persists in the high-temperature phase of sample (c) even if the speed of transformation of α-Fe to $D0_3$ structure is very high. For sample (d) with 46.1 at.% Al, the nanoparticles first have the α-Fe structure in a narrow temperature range between 1573 and 1593 K, and they change to B2 structure in equilibrium below 1573 K. Thus, it is easy for the nanoparticles to transform totally from α-Fe to pure B2 structure at high cooling rates. For sample (e) with 56.5 at.% Al, the final phase in equilibrium should be the FeAl and $FeAl_2$ intermetallics; however, B2 phase together with α-Fe are formed instead. Likewise, for sample (f), Al and an unidentified phase are produced in place of Al and Al_3Fe intermetallic. This indicates that the phase diagram for nanoparticles with high Al content is quite different from the equilibrium diagram at high cooling rates.

4. Conclusions

Fe–Al nanoparticles of eight kinds with particle size ranging from 29 to 46 nm were prepared successfully by HPMR. Nanoparticles containing Al have better oxidation resistance than pure Fe nanoparticles during passivation. The Al contents in Fe–Al UFPs are about 1.2–1.7 times those in the master alloys, increasing almost directly with the content of Al below 50 at.% in master alloys. With Al contents less than 25 at.% in bulk, the speed of evaporation of Fe in Fe–Al alloys is accelerated by addition of aluminium and likewise Al evaporation is enhanced by Fe with Al contents above 50 at.% in bulk.

The crystal structures of Fe–Al nanoparticles vary with the composition. As regards nanoparticles with 27.1 and 46.1 at.% Al, pure Fe_3Al and FeAl intermetallics are successfully produced, respectively. For Fe–Al nanoparticles with Al content over 56.5 at.%, the crystal structures of nanoparticles do not comply with the equilibrium phase diagram and no intermetallics form other than Fe_3Al and FeAl. HPMR is suitable for preparing ultrafine intermetallic compound particles at low cost.

Acknowledgments

This work was supported by the National Natural Science Foundation of China (Grants Nos 20025103, 20171002 and 50274002). The authors acknowledge Assistant Professor X Z Gai and Associate Professor F H Liao for their kind technical help with TEM and XRD measurements.

References

[1] Giri A K and Chakraborty D 1991 *Trans. Indian Ceram. Soc.* **50** 28
[2] Koster E 1993 *J. Magn. Magn. Mater.* **120** 1
[3] Ding J, Tsuzuki T, McCormick P G and Street R 1996 *J. Magn. Magn. Mater.* **162** 271
[4] Zhang L and Manthiram A 1996 *J. Appl. Phys.* **80** 4534
[5] Inoue A, Saida J and Masumoto T 1988 *Metall. Trans.* A **19** 2315
[6] Zhang H Y, Gu B X, Zhai H R and Lu M 1994 *Phys. Status Solidi* a **143** 399
[7] Livage J, Henry M and Sanchez C 1988 *Prog. Solid State Chem.* **18** 259
[8] Hahn H and Averback R S 1990 *J. Appl. Phys.* **67** 1113
[9] Ohno S and Uda M 1984 *Trans. Japan Inst. Met.* **48** 640
[10] Ohno S and Uda M 1989 *J. Japan Inst. Met.* **53** 946
[11] Li X G, Chiba A and Takahashi S 1997 *J. Magn. Magn. Mater.* **170** 339
[12] Li X G, Murai T, Aaito T and Takahashi S 1998 *J. Magn. Magn. Mater.* **190** 277
[13] Li X G and Takahashi S 2000 *J. Magn. Magn. Mater.* **214** 195
[14] Li X G, Murai T, Chiba A and Takahashi S 1999 *J. Appl. Phys.* **86** 1867
[15] Liu T, Shao H Y and Li X G 2003 *Intermetallics* at press
[16] Negri D, Yavari A R and Deriu A 1999 *Acta Mater.* **47** 4545
[17] Jartych E, Zurawicz J, Oleszak D and Pekala M 1998 *J. Phys.: Condens. Matter* **10** 4929
[18] Perez R J and Lavernia E 1998 *J. Mater. Sci. Eng.* A **255** 124
[19] Granqvist C G and Buhrman R A 1976 *J. Appl. Phys.* **47** 2200
[20] Liu T, Zhang Y H and Li X G 2003 *Scr. Mater.* **48** 403
[21] Massalski T B, Murray J L, Bennet L H, Baker H and Kacprzak L 1986 *Binary Alloy Phase Diagrams* (Metals Park, OH: American Society for Metals) p 112